Energy & Environmental Science

ROYAL SOCIETY OF CHEMISTRY

PAPER

View Article Online
View Journal | View Issue

Cite this: *Energy Environ. Sci.*, 2022, **15**, 2927

A sinter-free future for solid-state battery designs†

Zachary D. Hood, ‡[a] Yuntong Zhu, [a] Lincoln J. Miara, [ab] Won Seok Chang, [ac] Philipp Simons[a] and Jennifer L. M. Rupp *[ad]

Received 25th January 2022,
Accepted 7th June 2022

DOI: 10.1039/d2ee00279e

rsc.li/ees

Ceramic-based solid electrolytes and separators are particularly attractive for use in next-generation batteries as a way to increase the electrochemical stability window and improve safety. However, batteries with higher energy densities require thin membranes comparable in thickness to the polymer separators (*e.g.*, 10–25 μm) found in today's Lithium-ion batteries. To date, conventional ceramic–electrolyte processing routes have not been able to achieve this goal as they typically operate on the principle of sintering: going from particle to a densified ceramic body. To overcome this challenge, we provide a blueprint for an alternative cost-effective sequential decomposition synthesis (SDS) approach that uniquely accesses the thickness range required from solid Li oxide-based electrolytes close to those of today's polymer separators and offers immense opportunities for to obtain the desired phase at significantly lower processing temperatures (<700 °C) with unique ceramic microstructures. We specifically highlight the SDS processing of Li garnets and disclose basic SDS precursor and ceramic processing concepts that can be adapted to other Li-containing oxides.

Broader context

Next-generation Lithium (Li) metal batteries are essential for the paradigm shift from small power sources designed for portable electronics to large-scale energy storage devices for electric vehicles. Although these new battery designs request solid-state electrolytes comparable in thickness to the polymer separators found in today's Lithium-ion batteries, there are limited methods to fabricate oxide-based solid-state electrolytes with such dimensions. Here, we invented a new approach, termed Sequential Decomposition Synthesis (SDS), that uniquely accesses the thickness ranges of 1 – 10 μm for Li oxide-based solid-state electroyltes. Due to the wider electrochemical stability window of SDS-manufactured solid electrolytes like Li garnets and potential to integrate excess Li during the SDS process, this represents an important step to delivering cost-effective ceramic process alternatives toward established polymer battery separators. Additionally, the SDS method offers new options for future battery architectures and omits high-temperature sintering to enable the synthesis of new Li-electrolyte materials for which co-bonding or sintering at lower temperatures is challenging.

Introduction

The paradigm shift from small batteries designed for portable electronics to large-scale batteries for electric vehicles is a grand engineering challenge, with a goal of safely storing large amounts of electricity at a low cost, and enabling the shift from the use of fossil fuels to a carbon free mobility sector.[1–5] State-of-the-art lithium-ion batteries (LIBs), with liquid-based electrolytes, face numerous performance-related complications. For example, the Li-metal anode, having the highest electrochemical specific energy known for solids of 3860 mA h g^{-1},[6,7] cannot be used with traditional organic liquid electrolytes in LIBs because of poor performance and safety concerns. Recent progress in solid-state battery (SSB) electrolytes such as Li garnets (*e.g.*, $Li_{6.25}Al_{0.25}La_3Zr_2O_{12}$, LLZO) provide a promising alternative to liquid-based electrolytes with wide electrochemical stability (0.05 to ~4.7 V),[8,9] fast Li^+ conductivity in the mS cm^{-1} range under ambient conditions,[10,11] structural retention in the presence of water,[12] non-flammability,[13] and perhaps most importantly, compatibility with a Li–metal anode through the

[a] *Department of Materials Science and Engineering, Massachusetts Institute of Technology, Cambridge, MA 02139, USA. E-mail: jrupp@mit.edu*
[b] *Advanced Materials Lab, Samsung Semiconductor, Inc, Cambridge, MA, 02135, USA*
[c] *Samsung Advanced Institute of Technology (SAIT), Samsung Electronics Co., Ltd, Suwon, Korea*
[d] *Department of Electrical Engineering and Computer Science, Massachusetts Institute of Technology, Cambridge, MA 02139, USA*

† Electronic supplementary information (ESI) available: Materials and methods, Supplementary text, Fig. S1–S10, Movie S1 and S2. See DOI: https://doi.org/10.1039/d2ee00279e

‡ Present address: Applied Materials Division, Argonne National Laboratory, Lemont, IL, 60439, USA.

formation of a stable tetragonal-like interphase at the Li garnet/Li interface.[14–16] Nevertheless, two major challenges for Li-garnet electrolytes in SSBs are (i) their large-scale processability as technologically viable films close in thickness to polymer separators in LIBs (below 20 μm) and (ii) stabilization of the cubic, high-conductivity phase[11,17,18] as mechanically robust films.

In a solid-state battery, the electrolyte functions as both the separator and the medium for shuttling ions between the anode and cathode, and consequently, thicker solid electrolyte separators compromise the volumetric/gravimetric energy of the full cell. Thus, the exploration of feasible chemistries and processing techniques to produce dense Li^+-conducting solid separators between 1 and 20 μm thickness is not only missing from the literature but also deserves special attention from the field. In fact, looking at the techno-economics, it is clear that for a target price set by the U.S. Department of Energy of US$100 kW h^{-1}, 75% of the production costs may be overestimated due to the assumption that high-temperature sintering is required.[5] The main cost contributors to the SSB manufacturing depend critically on three factors, which, in the long run, need to be diminished: first, in any conventional sintering method the separate processing routes for powder synthesis and densification *via* sintering add unavoidable consecutive processing lines and complex machinery for powder synthesis, green body forming, and sintering to >1000 °C. Processes such as ''reactive sintering'' may be able to combine the formation of a green body with the synthesis/densification of ceramics, however, such processes generally yield ceramics that are thicker than 100 μm. Second, any sinter process ramps up the energy costs per kilogram of material processed for the SSB and typically requires a co-sinter strategy to assemble a tight electrolyte/cathode interface.[19] Such a co-sinter strategy would be a huge cost contributor and excludes many attractive cathode materials (*e.g.*, $LiFePO_4$, $LiNi_{0.8}Co_{0.15}Al_{0.05}O_2$, *etc.* as co-sinter temperatures with LLZO leads to the formation of insulating impurity phases).[19] Third, the alternative of processing thin films <1 μm in thickness resolves the first two concerns, as a successive powder synthesis-to-densification protocol is no longer a requirement and high-temperature co-sintering can be omitted; however, most established film depositions are based on vacuum technology, which adds to machine costs and challenges in scaling up production.[5] The most disruptive option to make future low-cost and mass-manufacturable SSB electrolytes as films of 1–20 μm in thickness is to redefine the chemistry and ceramic densification *via* wet-chemical routes and run counter to a ceramicist's best instincts: ''Ditch The Sintering''. It is surprising that a recent data-mining analysis of around 900 papers on the processing parameters of SSB electrolytes revealed that for Li garnets, no wet-chemical protocol has been developed that results in suitable Li conductivities at the projected thickness range and avoids a sintering route.[20]

More specifically, recent reports on SSB oxide film manufacturing indicate that these processes have been predominantly developed for the fabrication of thin-film Li garnets *via* vacuum-based techniques, including pulsed laser deposition (PLD),[21–23] radio frequency magnetron sputtering,[24–26] atomic layer deposition,[27] and chemical vapor deposition.[28–30] Even though most of these strategies can be optimized to achieve suitable conductivity and thicknesses between 40 and 700 nm,[18,31] these techniques require (i) a high vacuum environment and/or (ii) a relatively long processing duration (*e.g.*, pump-down, deposition, *etc.*), which collectively increase the cost for large-scale deployment of SSB electrolytes.[4,5,32] Although the pursuit of thin-film Li garnets with high Li^+ conductivity for next-generation batteries continues to gain momentum, industry demands inexpensive methods and machine lines that do not require high vacuum or, in some cases, long processing durations.

A suitable alternative for processing SSB electrolytes with a small form factor at lowered temperatures for SSBs that avoids classic powder-to-sinter routes for densification is the development of wet-chemical routes for chemistries such as Li garnets. Wet-chemical synthetic techniques offer a number of advantages compared with the state-of-the-art processing. First, more Lithium (Li) can be directly integrated into a solution and transferred to the solid during deposition compared with vacuum-based techniques. In addition, the manufacturing costs are low, and it is possible to directly deposit over wide areas. As recently discussed in a review[5] on thin robust SSB electrolyte manufacturing, turning to any wet-chemical processing with a direct solution-to-densification route using precursors (avoiding separate steps for particle preparation and sintering) requires a far more labor-intensive development process to define the precursor chemistry and control the stress evolution during drying and crystallization to produce crack-free and dense films when compared to established ceramic manufacturing routes through reactive sintering or vacuum-based growth. Wet chemical routes are often used in 1 or 2 cation oxides such as CeO_{2-x} and $Ce_{0.8}Gd_{0.2}O_{1.9-x}$,[33,34] but avoided in systems with many cations such as $Li_{6.25}Al_{0.25}La_3Zr_2O_{12}$ (LLZO) as it is difficult to produce single phase materials in high component systems. We attribute the underdevelopment of such wet-chemical processing routes for Li garnets, despite the technological attractiveness of such chemistries, to these challenges given the high cation and multiple bonding units.

We report a ceramic manufacturing method termed sequential decomposition synthesis (SDS), which results in ceramic films with thicknesses between 1 and 10 μm, while keeping the maximum process temperature to <700 °C.[35–37] To design such a ceramic processing route, we had to solve the existing problem of the thickness limitation (<1 μm) due to dry-crack evolution during the pyrolysis steps of film formation. This thickness limitation for pyrolysis-derived ceramics often stems from the phenomenon that all metal salts and organics decompose or evaporate during a single event close in temperature, leading to a large sudden mass loss, shrinkage, and cracking, analogous to auto-combustion in the Pechini method.[38] The SDS ceramic processing method proposed herein builds on having a rather wide range of soluble Li salts available that

decompose at potentially higher temperatures than many of the other metal–oxide-forming salts and on the ability of many Li-containing oxides to be processable at a relatively lower temperature. For instance, in SDS processing of Li garnets, one can exploit the ability of the approach to define two sets of decomposition events. In the first event, we can selectively bring only the non-Li cations, Al, Zr, and La, from a pyrolysis solution containing all the metal salts to an amorphous pyrochlore-like $La_2Zr_2O_7$ phase containing intact Li nitrate salt. This event can be followed by a second event, where we dissolve the Li salt at a higher temperature in the preformed $La_2Zr_2O_7$ pyrochlore phase.[39] The SDS process provides a new degree to separate the decomposition chemical reactions and control drying resulting in the ''sinter-less'' production of Li garnets and a uniquely high grain-to-film-thickness aspect ratios of around 80–500 that could prevent Li filament propagation and tune the electrochemical properties of the film.[5] Furthermore, the ''sinter-less'' densification of Li garnets at low temperatures using SDS enables the future integration of a wider range of cobalt-free cathodes such as $LiFePO_4$ or $LiNi_{0.5}Mn_{1.5}O_4$, as it matches their phase-stability requirements towards SDS-synthesized oxide electrolytes at low cost, as exemplified for LLZO. Another feature is the wider adaptability to establish excess Li in the ceramic synthesis to account for Li loss during heating; this Li can be directly transferred from a sprayed precursor solution into a densified film. This feature ensures an unusually high level of phase control at low temperatures that is difficult to achieve in classic calcination, sintering, or reactive sintering routes. This method is practical for both all-solid batteries and for use as an inorganic lithium stable separator in hybrid battery designs[40,41] with solid separators and liquid components enabling Li–metal anodes and high-voltage cathodes.

Results

Designing sequential decomposition synthesis process for four-cation Li-garnet ceramic electrolytes

In an SDS process to make Li-containing oxide films, one starts by defining a precursor chemistry containing a Li salt and the necessary metal salts for the target chemistry, dispersed in a high-boiling-point organic solution. The precursor solution is sprayed and transported as fine aerosol droplets to a heated substrate, where subsequent spreading and evaporation of the residual solvent occurs. Thus far, this process is in line with spray pyrolysis deposition in the ceramic literature[38] for non-Li-containing oxides, where now on the heated substrate, the pyrolysis chemical reactions would convert most of the metal salts into the oxide film in a single reaction. Unlike this classic pyrolysis technique geared toward the synthesis of ceramic thin films (<1 μm), we define for this new SDS thick film synthesis (>1–10 μm) a ''2-step pyrolysis reaction'' during solidification, nucleation, and growth to avoid rapid mass loss during the pyrolysis and control the drying. SDS consists of (i) a soluble Li salt precursor that decomposes at higher temperatures than the other metal–oxide-forming salts and (ii) the corresponding Li–oxide ceramic is processable at a lower temperature in its delithiated oxide phase, as shown in Fig. 1a. Sequentially, the undissolved Li salt can be decomposed and activated within the pre-formed SDS oxide film through further temperature increase, resulting in a dense and final Li-containing oxide composition. This second step is distinct from classic ''reactive sintering'' since SDS requires lower temperatures to decompose the Li salt and for annealing and densification of the film. The decomposition reaction and temperature choices defined in part by the precursor chemistry and the selection of metal salts and Li salts can be used to steer the 2-step reaction and control the drying at relatively low temperatures of <500 °C without the need for classic sintering for solidification. SEM in-plane and cross sections of SDS LLZO films show even coverage on the substrate, Fig. 1b and Fig. S1, S2 (ESI†). Comparison with established ceramic synthesis, Fig. 1c, shows that SDS is unique by separating in time and temperature the oxide backbone formation and the lithiation steps. This separation allows much thicker films to be formed than is typically seen with spray-pyrolysis. The power of splitting the reaction pathways during densification *via* SDS results in staggered control of the drying and sequenced stress adaption during phase formation, leading to unusually large thicknesses for a wet-chemically derived ceramic films compared to traditional ceramic process, Fig. 1d and e.

LLZO is particularly tricky to obtain since the crystal structure and film quality are sensitive to the Li concentration: if the Li concentration is too low the cubic phase cannot be achieved, if the Li concentration is too high the film quality degrades with the formation of porosity. In SDS processing of Li garnets, the first step decomposes $Zr(C_5H_7O_2)_4$, $Al(NO_3)_3{\cdot}9H_2O$, and $La(NO_3)_3{\cdot}6H_2O$ salts on contact with the heated substrate at 250–300 °C to induce 60 wt% of the total mass loss and yield a lithium nitrate rich amorphous phase in a pyrochlore-like matrix. In a second step, the film is heated to sequentially melt the amorphous Li nitrate phase, decompose the Li salt, crystallize the pyrochlore phase, and form the crystalline cubic Li garnet.

As the precursors have significant solubility in polar solvents such as methanol and poor solubility in most high-boiling-point solvents, we used a 1 : 1 : 1 solution by volume of methanol, 1-methoxy-2-propanol, and bis(2-ethylhexyl) phthalate, which are close to the decomposition points of the $Al(NO_3)_3{\cdot}9H_2O$, $La(NO_3)_3{\cdot}6H_2O$, and $Zr(C_5H_7O_2)_4$ salts and the Li-salt to be integrated into the solution at concentrations between 10 and 250 mol% in excess (see Table S1 ESI,† for chemistries). Additionally, 1-methoxy-2-propanol was used to increase the miscibility of methanol and bis(2-ethylhexyl) phthalate. This engineered SDS precursor solution does not reduce the metal salts and is stable for several weeks before any noticeable condensation or flocculation and is stable up to a concentration of 0.01 M (mol LLZO/L solvent). We indicate the decomposition temperature and solubility with color-coded simplification in the SDS precursor design by which (a) the pyrochlore-contributing metal-cation salts must be close in

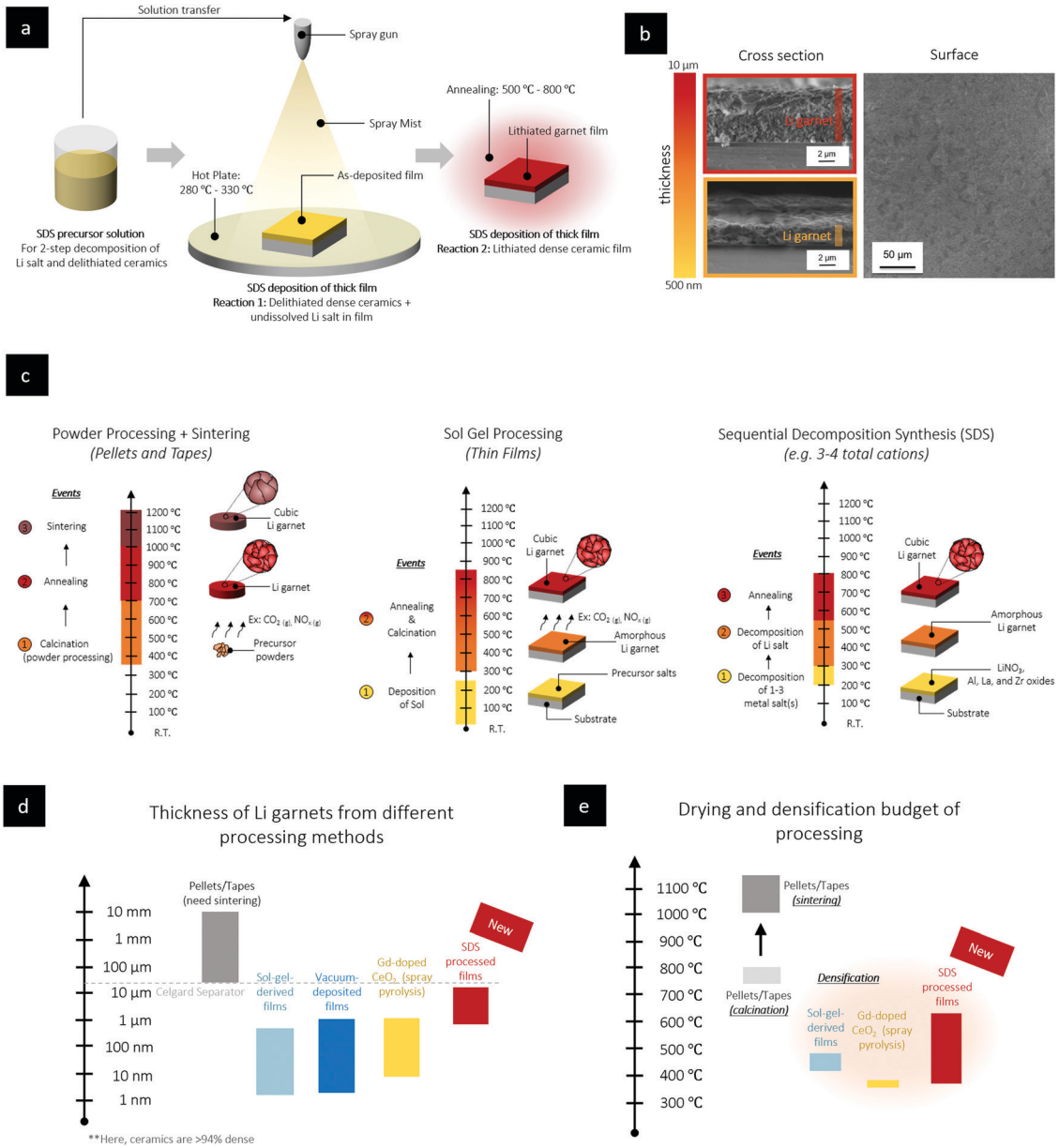

Fig. 1 Overview of sequential decomposition synthesis (SDS) processing. (a) Schematic representation of SDS processing, (b) SEM images of Li-garnet films processed *via* SDS (after annealing at spraying and after 750 °C under a flow of pure O_2), (c) processing temperature, events, and ionic conductivity of Li garnets synthesized *via* powder, sol-gel, and SDS processing. (d) Film thicknesses and E) drying and densification budget for processing Li garnets *via* SDS compared with those of other methods.

decomposition temperature (within the green shades, 300 °C) and (b) the Li–salt decomposition is at least 100 °C higher (within the yellow-orange or even red shades). Different organic solvents and atmospheres may be chosen, as different synthetic routes are highlighted in Fig. 2a and b.

LLZO thick films were deposited on (001)-oriented MgO substrates using the engineered precursor solutions of the SDS process and an initial deposition at 280–350 °C followed by annealing at 750 °C (ramp rate: 10 °C min^{-1}) under O_2 for crystallization, Fig. 2b. Employing SDS for the synthesis, we find that directly after deposition at a substrate temperature of 280–330 °C, most of the metal salts decompose to form an amorphous film together with preserved $LiNO_3$ at deposition. This result is corroborated by Raman spectroscopy (Fig. S3, ESI†), which shows the presence of near-order structure similar to that of pure $LiNO_3$ and an amorphous pyrochlore-like phase. X-Ray photoelectron spectroscopy (XPS) analysis of the as-deposited films clearly reveals the presence of nitrates in the as-deposited films, Fig. S4 (ESI†).

A unique modulation in thickness between 1 and 10 µm is revealed in the cross-sectional SEM images of SDS-processed Li garnets with dense microstructures, where we produce films with thicknesses of 1–2 µm and 5–7 µm, Fig. 2c. These thicknesses are nearly 10× higher than those of films grown using

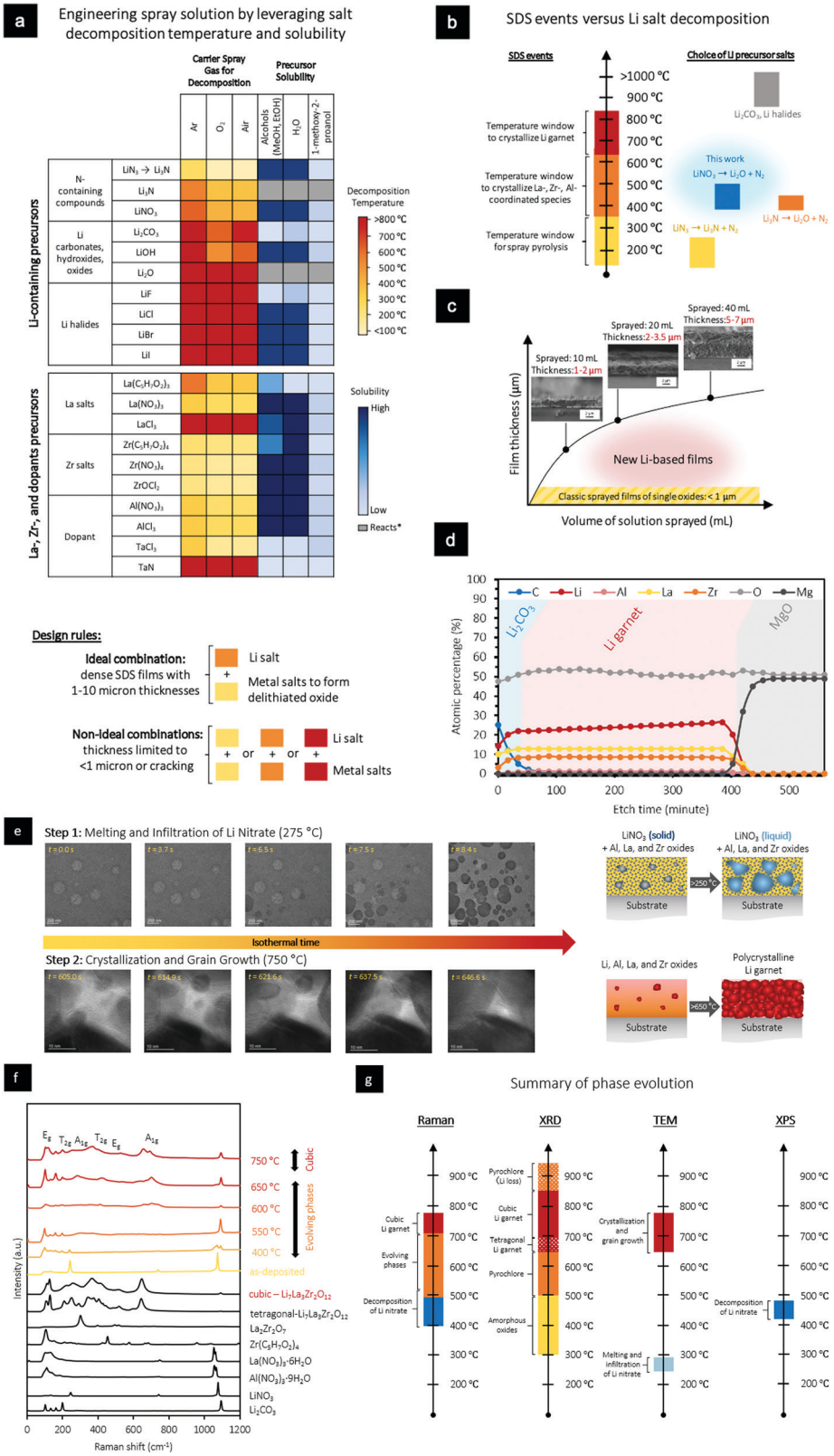

Fig. 2 Optimization of SDS procedures to form Li-garnet solid electrolytes. (a) Decomposition temperatures and solubility of precursor salts in the initial spray solution. (b) SDS events *versus* Li salt decomposition. (c) Thickness of Li garnet film as a function of volume of solution sprayed (75 mol% excess Li; insets show the cross section of noted films). (d) XPS depth profile of a sprayed Li garnet film (initial spray solution: 75 mol% excess Li). (e) *In situ* HR-TEM analysis displaying the melting and infiltration of Li nitrate into Al, La, and Zr oxides at 275 °C and crystallization and grain growth of Li-garnet films at 750 °C. Movies are provided in the ESI† Movies S1 and S2. These processes are didactically shown as an inset. (f) *In situ* Raman spectroscopy of the sprayed Li garnet films with 75 mol% excess Li. (g) Summary of phase evolution in light of Raman, XRD, TEM, and XPS results.

classic single cation-containing oxides. In fact, Fig. 2c shows the positive correlation between the solidified Li-ceramic film thickness and the amount of SDS solution sprayed for constant deposition temperatures of 280–330 °C and post-annealing at 750 °C. We performed XPS depth profiling using Ar^+ sputtering to further investigate the relative distribution of elements in the cross-section of a SDS post-processed film of LLZO (with 75 mol% excess Li). To obtain an averaged distribution of C, Li, Al, La, Zr, Mg, and O, we set the spot size to 400 μm for all the XPS depth profile experiments. Fig. 2d shows the XPS depth profile of a dense LLZO film with a known thickness of 4.5 ± 0.5 μm according to SEM analysis. As observed through Ar^+ depth profiling, the bulk of the film contained Li, Al, La, Zr, and O in relative atomic ratios similar to those of stoichiometric $Li_{6.25}Al_{0.25}La_3Zr_2O_{12}$. Importantly, there was no measurable Nitrogen in the film, signifying that all of the nitrate was decomposed during the annealing and solidification at 750 °C. To gain a more holistic understanding of the implication of excess lithiation on the phase, we turn to X-ray diffraction, Raman spectroscopy, and *in situ* TEM.

Evolution of phase and nanostructure in films grown *via* sequential decomposition synthesis

As evident in previous studies, the tetragonal phase of Li garnet has an overall lower ionic conductivity than that of the desired cubic phase.[42] To evaluate the long-range structural evolution of SDS-processed Li-garnet thick films, we used Raman spectroscopy with *in situ* heating to analyze the phases of an as-deposited film as a function of temperature and time, Fig. 2f. The as-deposited SDS films mainly showed Raman-active modes indicative of $LiNO_3$, as evident by the vibrational modes at 230 and 1150 cm^{-1}, together with an amorphous background that represents the formed oxide based on the decomposed La, Zr, and Al salts. Upon heating the film to 400 °C, several modes began to emerge at 100–220 cm^{-1} and 1080–1120 cm^{-1}, indicating an ongoing crystallization process with $La_2Zr_2O_7$ pyrochlore crystals forming as well as the decomposition of the Li nitrate salt. Upon heating the film to 600 °C, Raman vibrational modes began to form at 106 and 126 cm^{-1} (T_{2g}), 209 cm^{-1} (T_{2g}), 247 cm^{-1} (A_{2g}), and 288 cm^{-1} (T_{2g}), which can collectively be assigned to the tetragonal phase of LLZO and reveal the Li diffusion into the pyrochlore structure. Further heating the film to 750 °C causes the film to undergo a phase transition from the tetragonal to cubic garnet structure, as evident by the vibrational modes at 109 cm^{-1} (T_{2g}), 126 cm^{-1} (E_g), 255 cm^{-1} (A_{1g}), 365 cm^{-1} (T_{2g}), 420 cm^{-1} (T_{2g}), 517 cm^{-1} (E_g), and 665 cm^{-1} (A_{1g}). Heating the film to temperatures >850 °C causes Li loss and conversion of the components back into the $La_2Zr_2O_7$ pyrochlore phase, as indicated by *in situ* XRD (see Fig. S5, ESI†). These results are also corroborated by differential scanning calorimetry (DSC, Fig. S6, ESI†) analyses.

We leveraged the power of *in situ* HR-TEM with heating to better understand the reaction pathways and grain formation of LLZO films fabricated *via* SDS. For accurate TEM probing, thin films of 50–80 nm were directly deposited onto a Protochips Aduro chips using the SDS process, Fig. S7 (ESI†), and heated at a rate of 10 °C min^{-1} with isothermal dwells of 0.5–60 min between room temperature and 750 °C to evaluate the atomistic evolutions. Fig. 2e showcases two of the main processes observed during annealing of the SDS-synthesized films: (i) melting and infiltration of Li nitrate at 275 °C and (ii) crystallization and grain growth at 750 °C. As shown in Fig. 2e, a dense film of amorphous oxides with intact Li salt was deposited. The onset of melting and infiltration of Li nitrate into the film is a kinetically favorable process, occurring in as little as several seconds. Over time, Li nitrate uniformly wets the Al, La, and Zr oxide matrix. These results are in agreement with Raman results with *in situ* heating of as-deposited films of Li garnets, Fig. 2f. To investigate the effect of a second important event in the SDS synthesis, we heated the Li garnet film to 750 °C and probed the crystallization and grain growth *via in situ* HR-TEM. After isothermally heating the specimen at 750 °C for 605.0 s, several larger Li-garnet crystallites with an average size of >50 nm were observed, together with an amorphous matrix that shrank and was confined to amorphous grain boundaries over time, Fig. 2e. Within 10 s, pseudo-spherical nanocrystallites with diameters of 2–7 nm started to form within the amorphous grain boundary that continued to grow over 10–15 s. During this time, the larger grains continued to grow inward towards the amorphous grain boundary. Once the nanocrystallites came in contact with the larger grains, they were consumed within 5–20 s due to Ostwald ripening. During the subsequent 60 s, the larger grains continued to grow inwards towards the amorphous grain boundary, eventually forming a tight triple junction. It must be mentioned that the chemistry of the grain boundaries in films from SDS may be different from grain boundaries from sintered pellets and tapes of LLZO since increased temperatures (*e.g.*, >1000 °C) could cause possible elemental interdiffusion and/or segregation of dopants to the grain boundaries that would impact the electrochemical performance of the film.

In summary, by combining these observations, we present the microstructural evolution (Fig. 2e) and phase evolution (Fig. 2g) of an SDS-derived film, with the processing temperature, processing time, and major phases highlighted for clarity. As deposited, the films are composed of a homogenous distribution of $LiNO_3$ (solid) and an amorphous oxide of the Al, La, and Zr oxide constituents. When the temperature is ramped past 250 °C, the $LiNO_3$ melts to form an amorphous oxide with $LiNO_3$ (liquid). When the film is heated for 15–30 min between 525 and 650 °C, the $La_2Zr_2O_7$ pyrochlore phase emerges, see XRD results in Fig. S6 (ESI†). Upon heating to 650–750 °C, the cubic Li garnet crystallizes, forming classic grain–grain boundary structures of the ceramic film. Further heating the film past 850 °C for 1–30 min causes significant Li loss, yielding the $La_2Zr_2O_7$ phase.

Effect of lithiation on the microstructure and phase of Li-garnet films from sequential decomposition synthesis

It is known from earlier Li SSB science that fast-conducting electrolytes in particular require fine control of their lithiation in order to stabilize the desired phase.[5] This is often a

challenging process for all fabrication methods that involve sintering, since this step requires the addition of excess Li powder prior to sintering, or tightly controlling the Li partial pressure during sintering (due to the high volatility of Li). There is an existing limit on how much Li can be incorporated into a green ceramic body, as too high of a load, above 20 mol% for Li garnets, can result in crumbled and porous structures. In addition, it is well documented that Li loss in conventional thin-film techniques, such as PLD and RF sputtering, leads to the formation of mixed phases of tetragonal LLZO, cubic LLZO, and de-lithiated $La_2Zr_2O_7$, among various amorphous phases.[21] An interesting topic for SDS ceramic processing is to explore how much excess Li can be incorporated without damaging the densification process and drying.

What is the limit? And how does the decomposition of Li nitrate aid this type of ceramic synthesis? The effect of lithiation on the microstructure and phase of the films grown *via* SDS was explored. Because solution-based methods are amenable to directly integrating Li into the spray solution, we could easily tune the mol% of $LiNO_3$ in the spray solution to 10, 75, or 250 mol% excess Li and understand the role of excess Li on the microstructure and phase of the SDS-synthesized Li-garnet films. When 10 mol% excess Li was integrated into the precursor chemistry for the SDS process, SEM reveals that relatively smooth and dense films with thicknesses of 4.1 ± 0.9 μm together with a surface roughness (R_a) of ~0.4 μm, Fig. 3a. Incorporating 75 mol% excess Li into the precursor solution for SDS processing led to films with similar thicknesses (4.3 ± 1.0 μm); however, the R_a increased to ~1 μm and we measured ~15% porosity in the films. Further increasing the excess-Li to 250 mol% led to films with thicknesses of 4.4 ± 1.3 μm, R_a of ~3 μm, and large porosity in the film.

The Raman spectra confirmed that for 75–250 mol% excess Li in the SDS precursor, the resulting films after thermal annealing at 750 °C under O_2 retained a cubic structure, as indicated by the vibrational modes at 109 cm^{-1} (T_{2g}), 126 cm^{-1} (E_g), 255 cm^{-1} (A_{1g}), 365 cm^{-1} (T_{2g}), 420 cm^{-1} (T_{2g}), and 517 cm^{-1} (E_g), Fig. 3b and c. Decreasing the Li content in the initial spray solution to 10 mol% has a more significant impact on the phase of the film, resulting in mixed tetragonal-like garnet, as indicated by the vibrational modes at 209 cm^{-1} (T_{2g}), 247 cm^{-1} (A_{2g}), and 288 cm^{-1} (T_{2g}), and $La_2Zr_2O_7$ pyrochlore phases with vibrational modes at 290 and 450 cm^{-1}. We used electrochemical impedance spectroscopy (EIS) to measure the total conductivity of the films of the Li-garnet films processed *via* SDS, Fig. 3d. The films grown from an SDS precursor solution with 75 mol% excess Li showed the highest Li^+ conductivity of 2.4 ± 0.05 × 10^{-6} S cm^{-1} at 30 °C and 1.5 ± 0.05 × 10^{-4} S cm^{-1} at 185 °C, together with an activation energy of 0.34 ± 0.03 eV. These EIS results are within the same magnitude of many thin-film Li garnet electrolytes (see Fig. S10, ESI†), which are generally lower in ionic conductivity compared with bulk Li garnets from solid-state processing methods. In addition, the activation energies of the SDS films are comparable to bulk Li garnets, signifying that Li^+ migration is favorable in the SDS films. For films grown from solutions with 250 mol% excess Li, a drop in conductivity was measured, likely due to the pronounced pore evolution. The ionic conductivity was also lower for films that were grown with SDS precursor solutions with 30 mol% and 10 mol% excess Li.

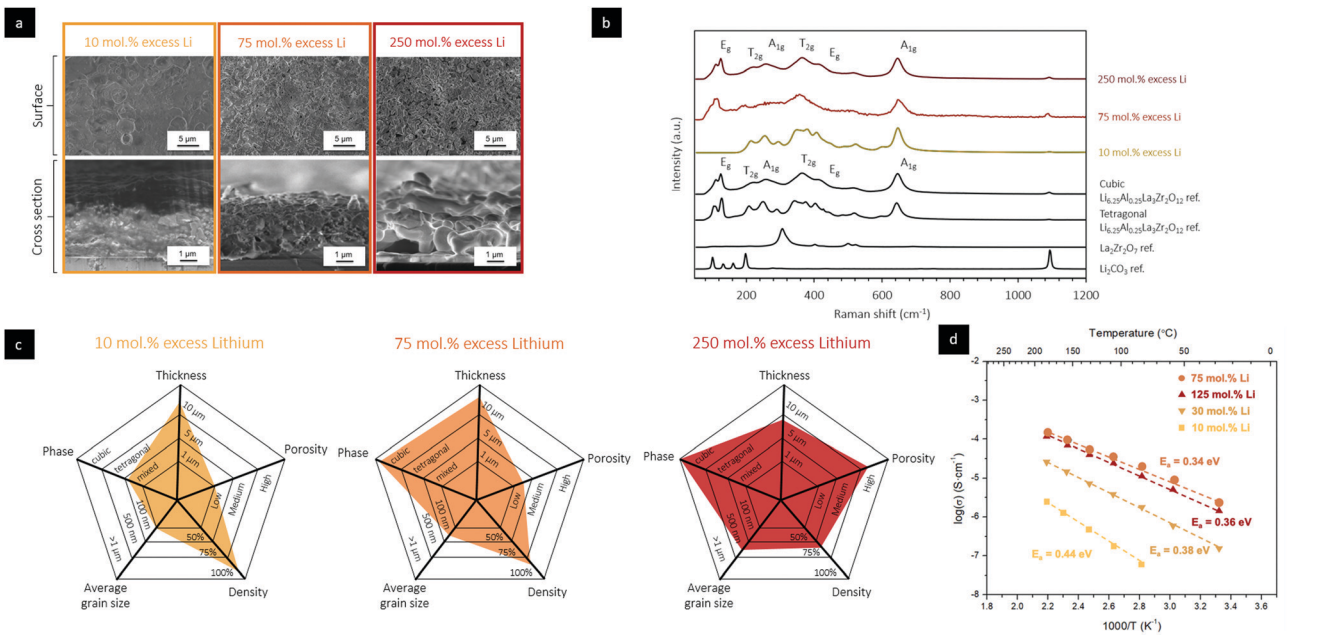

Fig. 3 Impact of lithiation on microstructure and electrochemical properties. (a) SEM micrographs of the surface and cross section of films grown by spray pyrolysis and annealed at 750 °C for 30 min under a flow of O_2. (b) Raman spectra of the sprayed films with different levels of lithiation (10, 75, and 250 mol% excess Li). (c) Spider plots depicting the thickness, porosity, density, average grain size, and phase of the Li-garnet films as a function of excess Li. (d) Arrhenius plot of the sprayed and post-processed films using 10–125 mol% excess Li in the initial spray solution.

Solutions with 10 mol% excess Li results in symmetry reduction to tetragonal-phase mixtures in a dense microstructure, which is associated with a conductivity drop (see Fig. S9 and S10, ESI†).

Several key conclusions can be drawn from these results. Tuning the stoichiometry of the SDS precursor solution to $\geq$75 mol% allows for crystallization of the desired cubic phase of the Li garnet and results in a thus far inaccessible thickness range of dense LLZO oxides of 1–10 μm without the use of sintering at relatively low temperatures and costs. This feature is attractive and indicates the potential of this alternative processing method for future solid electrolytes and separators for battery designs. Another interesting aspect is that by simply tuning the concentration of Li nitrate in the initial solution, the surface roughness and porosity can be readily altered in SDS-processed Li-garnet films. Such control over the surface roughness has obvious advantages in applications where one may want to tune the electrochemical surface area between the Li garnet and an electrode. We synthesized all the solid electrolyte structures here without sintering, which offers a level of simplicity to spray the separator and electrolyte simply on future cathodes or other support structures in battery design and avoid the thus-far-needed process of co-sintering to create strong mechanical bonds.

Conclusion

In summary, the SDS technique can be used to process Li garnets with thicknesses between 1 and 10 μm, close to the thicknesses of today's LIB polymer separators, without sintering. Due to the wider electrochemical stability window of SDS-manufactured solid electrolytes like Li garnets and potential to integrate excess Li, this is an important step to delivering cost-effective ceramic process alternatives toward established polymer separators. There are several other opportunities for future design and cost-competitiveness of SSBs stemming from the development of the SDS process. First, this process is notable because the classic ceramic manufacturing of solid electrolytes yields thick ($>$10 μm) solid electrolytes that require high sinter temperatures and strategies to bond at high temperatures with a cathode, whereby many attractive cobalt-free cathodes are unusable. Compared to earlier attempts of thin-film depositions, an alternative ceramic synthesis protocol is provided that overcomes the thickness limitation to go beyond the typical 1 μm without the need to use any pre-made particles (that later requiring sintering) and without an expensive vacuum machine park, as everything is synthesized from the wet stage. Second, we provide a proof-of-concept for the SDS ceramic processing of Li garnets with competitive thickness that possess unusually high grain-to-film-thickness aspect ratios around 80–500 and technologically viable Li^+ conductivities, all phase stabilized and processed at rather low temperatures. SDS, as a concept to design solution-based precursors and control decomposition routes, can be readily extended to a broad range of Li-containing oxides to stabilize desired phases at significantly lowered temperatures of more than 250 °C as it is no longer a particle-sintering densification route but starts from the wet phase. This feature is relevant for any future SSB design involving oxides for either the electrolyte or cathode, as it allows SDS spraying of the bilayer assembly or fabrication of one of the SSB constituents and SDS deposition of the other, thereby reducing existing restrictions of classic high-temperature co-sintering required to ensure mechanically stable bonds but often with the trade-off of decreased material selection due to phase instabilities.

Current prismatic cell-to-module and also more recently proposed blade battery cell-to pack batteries are designed for separators of 30 × 10 cm^2 or even 60 × 250 cm^2 for the automotive industry.[43] For the ceramics industry, it took decades to establish protocols detailing how to synthesize tapes with wide areas of max. 20 × 20 cm^2 defect-free *via* sintering for one of the best investigated ceramics like Al_2O_3.[44] The fact that tapes of 5 × 5 cm^2 for Li-garnet ceramic separators have been developed in a decade is promising, however, it remains to be proven whether these can be equally upscaled in area like alumina for EV battery packs. The development of the SDS ceramic manufacturing routes for Li-garnets was developed in an effort to provide potential alternative to classic tape and sinter manufacture, that may provide a higher potential with future process engineering adaptions to coat larger areas for battery EV packs. Cleary, this SDS method helps close the existing gap between the thicknesses of solid-oxide electrolytes and those of the polymer separators in current LIBs but with new options to integrate high-capacity Li anodes in the future. In addition, it omits high-temperature sintering to enable the wider integration of attractive lower-temperature-phase-stable cathodes or synthesis of new Li-electrolyte materials for which co-bonding or sintering at lower temperatures is challenging.

Author contributions

Z. D. H. and J. L. M. R. initiated and developed the SDS process concept for Li ceramics and the basic design of the experiments. Z. D. H., Y. Z., and J. L. M. R. developed the SDS precursor chemistry for the spray solutions. P. S. and J. L. M. R. designed and constructed the SDS-ceramic synthesis chamber. P. S., J. L. M. R., and Z. D. H. developed an SDS prototype machine. Z. D. H., Y. Z., and W.-S. C. completed the experiments, and L. M. and P. S. supported the analysis of the data. All the authors contributed to the research and discussion of the data, figure preparation, and proofreading of the manuscript. Z. D. H. and J. L. M. R. contributed to the writing and editing of all the manuscript sections.

Conflicts of interest

The authors declare no conflicts of interest.

Acknowledgements

This research was supported by Samsung Electronics. A portion of this research was conducted at the Center for Nanophase Materials Sciences, which is a DOE Office of Science User Facility.

References

1 B. Obama, The irreversible momentum of clean energy, *Science*, 2017, **355**, 126–129.
2 N. J. Dudney, W. C. West and J. Nanda, *Handbook of Solid State Batteries*, World Scientific, 2016.
3 J. Janek and W. G. Zeier, A solid future for battery development, *Nat. Energy*, 2016, **500**, 300.
4 Y. Zhu, *et al.*, Solid state lithionics: Lithium film ceramics towards future functionalities, *Nat. Rev. Mater.*, 2020, 1–19.
5 M. Balaish, *et al.*, Processing thin but robust electrolytes for solid-state batteries, *Nat. Energy*, 2021, 1–13.
6 W. Xu, *et al.*, Lithium metal anodes for rechargeable batteries, *Energy. Environ. Sci.*, 2014, **7**, 513–537.
7 D. Lin, *et al.*, Reviving the lithium metal anode for high-energy batteries, *Nat. Nanotechnol.*, 2017, **12**, 194.
8 T. Thompson, *et al.*, Electrochemical window of the Li-ion solid electrolyte $Li_7La_3Zr_2O_{12}$, *ACS Energy Lett.*, 2017, **2**, 462–468.
9 F. Han, *et al.*, Electrochemical stability of $Li_{10}GeP_2S_{12}$ and $Li_7La_3Zr_2O_{12}$ solid electrolytes, *Adv. Energy Mater.*, 2016, **6**, 1501590.
10 V. Thangadurai, *et al.*, Garnet-type solid-state fast Li ion conductors for Li batteries: critical review, *Chem. Soc. Rev.*, 2014, **43**, 714–4727.
11 R. Murugan, *et al.*, Fast lithium Ion conduction in garnet-type $Li_7La_3Zr_2O_{12}$, *Angew. Chem., Int. Ed.*, 2007, **46**, 7778–7781.
12 X. Liu, *et al.*, Elucidating the mobility of H^+ and Li^+ ions in $(Li_{6.25-x}H_xAl_{0.25})La_3Zr_2O_{12}$ *via* correlative neutron and electron spectroscopy, *Energy Environ. Sci.*, 2019, **12**, 945–951.
13 R. Li, *et al.*, Morphosynthesis of 3D macroporous garnet frameworks and perfusion of polymer-stabilized Lithium salts for flexible solid-state hybrid electrolytes, *Adv. Mater. Interfaces*, 2019, **6**, 1900200.
14 A. Sharafi, *et al.*, Characterizing the Li–$Li_7La_3Zr_2O_{12}$ interface stability and kinetics as a function of temperature and current density, *J. Power Sources*, 2016, **302**, 135–139.
15 A. Sharafi, *et al.*, Impact of air exposure and surface chemistry on Li-$Li_7La_3Zr_2O_{12}$ interfacial resistance, *J. Mater. Chem. A*, 2017, **5**, 13475–13487.
16 C. Ma, *et al.*, Interfacial stability of Li metal-solid electrolyte elucidated via in situ electron microscopy, *Nano Lett.*, 2016, **16**, 7030–7036.
17 J. Awaka, *et al.*, Crystal structure of fast lithium-ion-conducting cubic $Li_7La_3Zr_2O_{12}$, *Chem. Lett.*, 2010, **40**, 60–62.
18 R. Pfenninger, *et al.*, A low ride on processing temperature for fast lithium conduction in garnet solid-state battery films, *Nat. Energy*, 2019, **4**, 475–483.
19 K. J. Kim and J. L. M. Rupp, All ceramic cathode composite design and manufacturing towards low interfacial resistance for garnet-based solid-state lithium batteries, *Energy Environ. Sci.*, 2020, **13**, 4930–4945.
20 R. Mahbub, *et al.*, Text mining for processing conditions of solid-state battery electrolyte, *Electrochem. Commun.*, 2020, **121**, 106860.
21 I. Garbayo, *et al.*, Glass-type polyamorphism in Li-garnet thin film solid state battery conductors, *Adv. Energy Mater.*, 2018, **8**, 1702265.
22 P. Jung Hoon, *et al.*, Aluminum migration during deposition of $Li_7La_3Zr_2O_{12}$ thin Films on aluminum oxide substrates, *ECS Trans.*, 2013, **53**, 1–4.
23 T. Jiajia and A. Tiwari, Fabrication and characterization of $Li_7La_3Zr_2O_{12}$ thin films for Lithium ion battery, *ECS Solid State Lett.*, 2012, **1**, Q57–Q60.
24 S. Lobe, *et al.*, Radio frequency magnetron sputtering of $Li_7La_3Zr_2O_{12}$ thin films for solid-state batteries, *J. Power Sources*, 2016, **307**, 684–689.
25 N. Jian, *et al.*, Properties and preparation of Li–La–Ti–Zr–O thin film electrolyte, *Mater. Lett.*, 2015, **154**, 167–169.
26 M. Rawlence, *et al.*, Effect of gallium substitution on Lithium-ion conductivity and phase evolution in sputtered $Li_{7-3x}Ga_xLa_3Zr_2O_{12}$ thin films, *ACS Appl. Mater. Interfaces*, 2018, **10**, 13720–13728.
27 E. Kazyak, *et al.*, Atomic layer deposition of the solid electrolyte garnet $Li_7La_3Zr_2O_{12}$, *Chem. Mater.*, 2017, **29**, 3785–3792.
28 C. Loho, *et al.*, Garnet-type $Li_7La_3Zr_2O_{12}$ solid electrolyte thin films grown by CO_2-laser assisted CVD for all-solid-state batteries, *J. Electrochem. Soc.*, 2017, **164**, 6131–6139.
29 H. Katsui and T. Goto, Preparation of cubic and tetragonal $Li_7La_3Zr_2O_{12}$ film by metal organic chemical vapor deposition, *Thin Solid Films*, 2015, **584**, 130–134.
30 H. Katsui and T. Goto, Impedance of cubic $Li_7La_3Zr_2O_{12}$ film deposited on strontium ruthenate substrate by chemical vapor deposition, *Mater. Today: Proc.*, 2017, **4**, 11445–11448.
31 J. Sastre, *et al.*, Lithium garnet $Li_7La_3Zr_2O_{12}$ electrolyte for all-solid-state batteries: closing the gap between bulk and thin film Li-ion conductivities, *Adv. Mater. Interfaces*, 2020, **7**, 2000425.
32 J. Schnell, *et al.*, Prospects of production technologies and manufacturing costs of oxide-based all-solid-state lithium batteries, *Energy Environ. Sci.*, 2019, **12**, 1818–1833.
33 J. L. M. Rupp, *et al.*, Chemical analysis of spray pyrolysis gadolinia-doped ceria electrolyte thin films for solid oxide fuel cells, *Chem. Mater.*, 2007, **19**, 1134–1142.
34 J. L. M. Rupp and L. J. Gauckler, Microstructures and electrical conductivity of nanocrystalline ceria-based thin films, *Solid State Ionics*, 2006, **177**, 2513–2518.
35 Y. Zhu, Z. D. Hood, J. L. M. Rupp and L. J. Miara, *Solution-processed solid-state electrolyte and method of manufacture thereof, US Pat.*, 11251460, 2022.
36 Y. Zhu, Z. D. Hood, J. L. M. Rupp and L. J. Miara, *Solid-state electrolyte and method of manufacture thereof, US Pat.*, 11223066, 2022.
37 W. S. Chang, Z. D. Hood, J. L. M. Rupp and L. Miara, *Amorphous nitrogen-rich solid state lithium electrolyte, US Pat.*, 17/115152, 2022.

38 D. Perednis and L. J. Gauckler, Thin film deposition using spray pyrolysis, *J. Electroceram.*, 2005, **14**, 103–111.
39 J. M. Weller and C. K. Chan, Pyrochlore nanocrystals as versatile quasi-single-source precursors to lithium conducting garnets, *J. Mater. Chem. A*, 2020, **8**, 17405–17410.
40 J. Liu, *et al.*, The interface between Li6.5La3Zr1.5Ta0.5O12 and liquid electrolyte, *Joule*, 2020, **4**, 101–108.
41 A. Gupta, *et al.*, Electrochemical and surface chemistry analysis of Lithium lanthanum zirconium tantalum oxide (LLZTO)/liquid electrolyte (LE) interfaces, *J. Power Sources*, 2020, **474**, 228598.
42 E. Rangasamy, *et al.*, Role of Al and Li concentration on the formation of cubic garnet solid electrolyte of nominal composition $Li_7La_3Zr_2O_{12}$, *Solid State Ionics*, 2012, **206**, 28–32.
43 ''The Next-Generation Battery Pack Design: from the BYD Blade Cell to Module-Free Battery Pack'', **https://medium.com/batterybits/the-next-generation-battery-pack-design-from-the-byd-blade-cell-to-module-free-battery-pack-2b507d4746d1**, accessed 18 May 2021.
44 Personal communications with industry, JLM Rupp. May 2021.